International Journal of Nanomedicine

Dovepress
Taylor & Francis Group

Open Access Full Text Article

ORIGINAL RESEARCH

ROS-Sensitive $MgOSiO_2$ Nano Capsules for Effective Against Osteoarthritis in Rat Model

Yu Zheng[1,*], Zhouxiaolong Zhang[2,*], Yingna Cui[3], Na Liu[1], Hongting Ma[2], Benjie Wang[1], Ruixin Li[1], Nan Zhu[2], Nan Zhang[1]

[1]Department of Orthopedics, The Affiliated Xinhua Hospital of Dalian University, Dalian, Liaoning Province, People's Republic of China; [2]School of Chemistry, Dalian University of Technology, Dalian, Liaoning Province, People's Republic of China; [3]School of Chemistry, Dalian University, Dalian, Liaoning Province, People's Republic of China

*These authors contributed equally to this work

Correspondence: Nan Zhang; Nan Zhu, Email zhn1979-08@163.com; nanzhu@dlut.edu.cn

Introduction: Magnesium oxide nanoparticles (MgO NPs) as magnesium ionophores have shown potential as a therapeutic strategy for osteoarthritis. However, the rapid absorption and clearance of MgO NPs in the joint cavity and the lack of a clear underlying mechanism may limit their therapeutic efficacy.

Methods: $MgO@SiO_2$ nano capsules were synthesized as a controlled-release nanosystem to mitigate the rapid clearance and potential toxicity of MgO NPs. The physicochemical properties and surface charge of the nano capsules were examined through TEM, EDS, XRD and Zeta potential. The kinetics of nano capsule degradation were measured using using inductively coupled plasma optical emission spectrometry and pH monitoring both in vivo and in vitro. Cytotoxicity and reactive oxygen species (ROS) were monitored to assess the dose-dependent effect of $MgO@SiO_2$ on ROS-mediated oxidative stress. Finally, ROS production and the expression of proinflammatory factors (IL-6, MMP-13, COX-2) were quantified in the cartilage of osteoarthritis samples to evaluate the potential mechanism of action of the nanocapsules for treating osteoarthritis.

Results: $MgO@SiO_2$ nano capsules extended the duration of MgO NPs release from 12 h to 3–5 days both in vivo and in vitro. $MgO@SiO_2$ exhibited no cytotoxicity toward chondrocytes at formula concentrations <15 mM. Notably, low concentrations (5 mM) of $MgO@SiO_2$ (and thus of MgO NPs) suppressed ROS generation in chondrocytes, whereas higher concentrations (>10 mM) increased ROS production. In a rat model of osteoarthritis, intra-articular injection of 5 mM $MgO@SiO_2$ samples significantly alleviated cartilage degeneration and destruction. Finally, ROS levels and the expression of certain proinflammatory factors (IL-6, MMP-13, COX-2)] in articular cartilage were markedly reduced.

Conclusion: As a multi-functional ROS-responsive nanosystem, $MgO@SiO_2$ nano capsules not only slow the release of MgO NPs and reduce their cytotoxicity but also reduce ROS production and thus lessen the inflammatory response in cartilage. This dual-action mechanism achieves therapeutic efficacy for osteoarthritis, offering a promising strategy to delay or reverse osteoarthritis progression.

Keywords: ROS-responsive nanosystem, $MgO@SiO_2$ nanocapsules, antioxidative stress, osteoarthritis

Introduction

Osteoarthritis (OA) is a prevalent chronic degenerative disease characterized by articular cartilage degeneration, subchondral sclerosis, synovial inflammation, and structural alterations in periarticular tissues, including the joint capsule, ligaments, and muscles.[1] Globally, OA affects approximately 7.6% of the population and ranks among the leading causes of adult disability, with its burden escalating steadily.[2] Pathologically, OA is a multifactorial disorder driven by the overproduction of reactive oxygen species (ROS) triggered by senescence, mechanical stress, and over-production of inflammatory cytokines.[3,4] ROS accumulation damages lipids, proteins, and DNA, inducing ferroptosis, apoptosis, and necrosis in chondrocytes.[5] Consequently, restoring ROS homeostasis in chondrocytes has emerged as a potential therapeutic strategy, spurring research into novel antioxidative strategies.

Received: 9 June 2025
Accepted: 5 September 2025
Published: 14 September 2025

Graphical Abstract

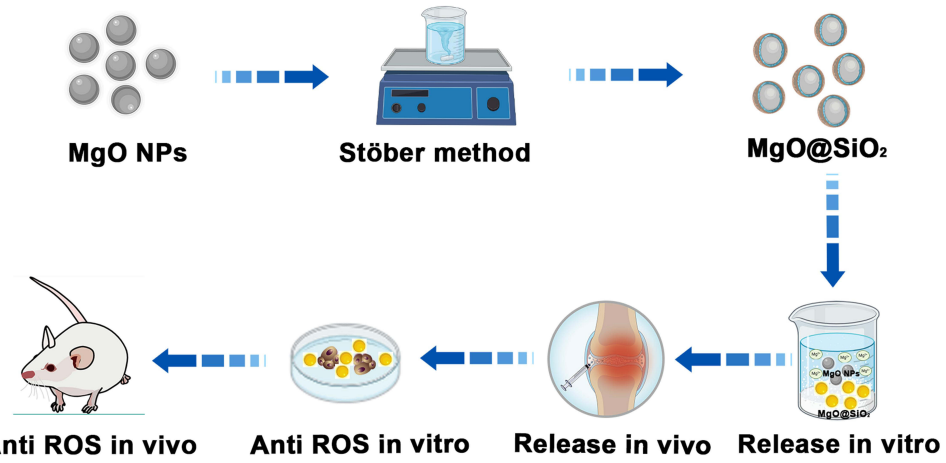

In recent years, with the development of nanotechnology, nano materials that are tailored to alleviate oxidant stress have become an attractive option for OA treatment. Nano antioxidative stress therapy not only leverages the unique physical, chemical and biological properties of nanomaterials, such as large specific surface area and good biocompatibility, but also has the advantage of targeted delivery of a drug(s) to the diseased site, regulated drug release, reduced systemic side effects, and improved therapeutic effect.[6] Studies have shown that nanoparticles (NPs) prepared by encapsulating metal ions (Li, Au),[7,8] bilirubin,[9] or a traditional Chinese medicine (curcumin, resveratrol, etc.)[10] with liposomes or nanomaterials can effectively relieve cartilage damage and improve joint function. As such, nano antioxidant therapy has emerged as a potential therapeutic strategy for OA and other disorders associated with imbalances in redox signaling.

The magnesium ion (Mg^{2+}) is an important trace element in humans, with substantial protective effects on cartilage. Mg^{2+} not only directly promotes the proliferation and differentiation of chondrocytes but also promotes the synthesis of cartilage matrix by upregulating the expression of chondroblast-specific genes and enhancing collagen production, and thus Mg^{2+} plays a key role in maintaining homeostasis in articular cartilage.[11] Conversely, Mg^{2+} deficiency promotes OA progression by promoting the release of inflammatory mediators, calcification of cartilage, and sensitization to pain signaling.[12] Clinically, intra-articular injection of $MgCl_2$ or $MgSO_4$ has been used to relieve OA inflammation and pain.[13,14] Mechanistically, Mg^{2+} exhibits antioxidative effects by binding to electronegative atoms (O, N) in ribosomes and polynucleotides, thus shielding DNA and RNA from ROS damage.[15] It also suppresses mitochondrial ROS production by downregulating components of the electron transport chain (eg, NDUFB6, SDHC, ATP5F1),[16] inhibiting phagocytic respiratory bursts,[17] and competitively blocking Ca^{2+}-mediated mitochondrial oxidative/nitrosative stress.[18] Notably, administration of supplemental Mg^{2+} to target tissues has been shown to mitigate ROS-driven chondrocyte damage comparably with the mitochondrial ROS scavenger mito-TEMPO,[19] highlighting the therapeutic promise of Mg^{2+} supplementation.

Magnesium oxide NPs (MgO NPs), as Mg^{2+} carriers, address key pharmacokinetic limitations of conventional magnesium salts. Their high surface area-to-volume ratio enhances Mg^{2+} loading capacity, while their cationic surface facilitates electrostatic targeting of negatively charged cartilage, enabling deep penetration into the extracellular matrix and subsequent intracellular Mg^{2+} release. Additionally, MgO NPs have been reported to promote the proliferation and differentiation of osteoblasts by curtailing the production of ROS.[20] Our previous studies showed that, compared with the administration of $MgCl_2$, MgO NPs could effectively prolong the release time of Mg^{2+} and significantly inhibit the cartilage damage of OA, and this effect increases with the increase of NP size.[21] Therefore, MgO NPs not only release Mg^{2+} slowly to exert its physiological functions but also have the ability to inhibit cartilage degeneration, which

undoubtedly helps to alleviate the pathological processes of OA. However, oral or systemic systemic administration of MgO NPs also faces challenges similar to those of Mg^{2+} salts, including poor gastrointestinal absorption and rapid intra-articular clearance, necessitating frequent high-dose administration that risks local toxicity and reduces patient compliance.

To overcome these limitations, we previously developed a MgO@SiO_2 core-shell nanocapsule system in which a silica (SiO_2) coating stabilizes MgO NPs and enables sustained Mg^{2+} release in vitro, thereby enhancing anti-inflammatory effects and cartilage repair in patient samples.[22] Despite these advances, the antioxidative mechanisms of MgO@SiO_2 in OA remain poorly defined. Therefore, we investigated the concentration of MgO@SiO_2 nano capsules necessary to counter ROS production in OA chondrocytes, evaluated their in vivo degradation kinetics in the joint cavity microenvironment for the first time, and further studied their therapeutic [efficacy for reducing oxidative stress and limiting OR efficacy for reestablishing oxidative homeostasis and limiting the inflammatory response in cartilage. Our goal was to bridge critical gaps in our understanding of the mechanisms by which MgO@SiO_2 nano capsules counter the deleterious effects of ROS, providing a foundation for clinical translation to OA treatment strategies.

Materials and Methods

Synthesis of MgO@SiO_2 Nano Capsules

MgO@SiO_2 nano capsules were synthesized by the Stöber method.[22] Briefly, 10 mg MgO NPs (Sigma-Aldrich, USA) were dispersed in a solution containing 5 mL ethanol and 0.2 mL of 28% ammonium. The mixture was stirred at room temperature for 30 min to ensure homogeneity. Subsequently, 90 µL tetraethyl orthosilicate (Sigma-Aldrich, USA) was added dropwise (1 drop over 5 s) under continuous stirring, and the reaction was allowed to proceed for 24 h. The resulting nano capsules were collected by centrifugation at 6000 rpm for 10 min, followed by repeated washing cycles with anhydrous ethanol to remove unreacted precursors. Finally, the purified MgO@SiO_2 nano capsules were stored for further characterization.

Characterization

The morphology and elemental composition of MgO NPs and MgO@SiO_2 nanocapsules were analyzed using transmission electron microscopy (TEM; JEM-F200, JEOL, Japan) coupled with energy-dispersive X-ray spectroscopy (EDS). Samples for TEM were prepared by dispersing NPs in ethanol, followed by sonication (30 min) and deposition onto carbon-coated copper grids. The average NP size of samples was calculated by applying Image J software V1.8.0.112 (NIH, USA) to TEM images. Phase composition was determined by X-ray diffraction (SmartLab, Rigaku, Japan) with Cu Kα radiation (λ = 1.5406 Å) at 40 kV and 40 mA. The Zeta potential [(ζ)] of MgO NPs and of MgO@SiO_2 nano capsules was measured in anhydrous ethanol using a Litesizer 500 (Anton Paar, Austria) at 25°C, with triplicate measurements per sample to ensure reproducibility.

Mg^{2+} Quantification

For Mg^{2+} quantification, 1 mg MgO NPs or MgO@SiO_2 nano capsules was fully digested in 5 mL concentrated HNO_3 (65%) at 80°C for 2 h. The resulting solution was diluted to 500 mL with deionized water (18.2 MΩ·cm resistivity) to achieve a homogeneous mixture. Mg^{2+} concentration was measured using inductively coupled plasma optical emission spectrometry (ICP-OES; Avio 500; PerkinElmer, USA) with a calibration curve generated from standard Mg^{2+} solutions (0.1–100 ppm, $R^2 > 0.999$). The actual MgO content in NPs and nanocapsules was calculated stoichiometrically based on the measured Mg^{2+} concentration, accounting for the molecular weight ratio of MgO (40.3 g/mol) to Mg (24.3 g/mol). Triplicate measurements were performed, with relative standard deviations of <2%.

Drug Release Assessment

Samples containing 10 mM Mg^{2+} equivalent of either MgO NPs or MgO@SiO_2 nanocapsules were immersed in 10 mL phosphate-buffered saline (PBS, pH 7.4) and incubated at 37 ± 0.5°C under constant agitation (100 rpm) using a thermostatic orbital shaker. The pH evolution of the release medium was monitored at predetermined times (0.5, 1,

3, 6, and 12 h; 1, 3, and 5 days) to indirectly assess Mg^{2+} release profiles. All experiments were conducted in triplicate under aseptic conditions.

For direct quantification of Mg^{2+} release kinetics, equivalent Mg^{2+} amounts (10 mM) of MgO NPs or MgO@SiO_2 nano capsules were separately loaded into dialysis tubing (3.5 kDa molecular weight cut-off) containing 10 mL deionized water. The sealed dialysis systems were maintained at 37 ± 0.5°C with gentle agitation (50 rpm) in a water bath over 7 days. Aliquots (200 μL) were periodically withdrawn from the external solution at designated time points (6 and 12 h; 1, 3, 5, and 7 days), diluted to 2 mL with deionized water, and analyzed using ICP-OES. The sampled volume was immediately replaced with fresh medium to maintain sink conditions. Three independent replicates were performed for each experimental group.

Isolation and Culture of Chondrocytes

Primary chondrocytes were isolated from articular cartilage of 4-week-old male C57BL/6 mice (Animal Laboratory Center, Xinhua Hospital, Dalian University; ethics approval no. 2023–04-01). Cartilage tissues were dissected from femoral heads and knee joints under sterile conditions, minced into 1–2 mm^3 fragments, and subjected to sequential enzymatic digestion. First, fragments were treated with 0.25% trypsin-EDTA (Gibco, USA) at 37°C for 30 min to remove residual soft tissue. After centrifugation (300 × *g*, 5 min), the supernatant was discarded, and the pellet was incubated in Dulbecco's Modified Eagle Medium (DMEM; HyClone, USA) containing 0.2% collagenase II (Gibco) at 37°C for 4 h under gentle agitation. The resulting cell suspension was filtered through a 70 μm nylon mesh (Corning, USA) to remove undigested debris, centrifuged (200 × *g*, 10 min), and resuspended in complete culture medium: DMEM supplemented with 10% heat-inactivated fetal bovine serum (FBS; Gibco), 1% penicillin-streptomycin (HyClone), and 2 mM L-glutamine (Gibco). Cells were seeded into T75 culture flasks (Corning) and maintained at 37°C in a humidified 5% CO_2 incubator (Thermo Scientific, USA), with medium refreshed every 48 h. Chondrocytes from passages 2–3 were used for experiments to ensure phenotypic stability. All procedures adhered to Guide for the Care and Use of Laboratory Animals for animal research reporting.

CCK-8 Assay

Primary chondrocytes (passages 2–3) were seeded into 96-well plates at a density of 1×10^4 cells per well in 100 μL complete medium and allowed to adhere for 24 h under standard culture conditions (37°C, 5% CO_2, humidified atmosphere). Cells were then exposed to fresh serum-containing medium supplemented with MgO NPs or MgO@SiO_2 nanocapsules at Mg^{2+} equivalent concentrations of 5, 10, or 15 mM. Untreated cells and medium-only wells served as negative and blank controls, respectively. After 24 h incubation, 10 μL of Cell Counting Kit-8 solution (CCK-8; C0038; Beyotime, China) was added to each well, followed by additional incubation for 2 h under standard culture conditions. Absorbance was measured at 450 nm with a reference wavelength of 650 nm using a microplate reader (Bio-Rad 680, Hercules, CA).

$$V_{viability} = (V_{sample} - V_{blank}) / (V_{control} - V_{blank}) \times 100\%$$

All experiments included six technical replicates per condition and were repeated independently three times. NP suspensions were sonicated (40 kHz, 5 min) before application to ensure dispersion homogeneity. Potential optical interference from NPs was excluded by parallel measurement of particle-containing medium without cells.

Intracellular ROS Quantification

Primary chondrocytes (passages 2–3) were seeded in 6-well plates at 4×10^5 cells per well and cultured to 80% confluency in complete medium under standard conditions (37°C, 5% CO_2, humidified atmosphere). To establish an in vitro OA model, cells were stimulated with 10 ng/mL IL-1β (PeproTech, USA) in serum-free DMEM for 24 h. Experimental groups were then treated with MgO NPs or MgO@SiO_2 nano capsules at Mg^{2+} concentrations of 5, 10, or 15 mM in serum-containing medium; IL-1β-stimulated cells served as OA controls and untreated cells as blanks. After 24 h incubation, cells were washed twice with warm PBS and loaded with 10 μM 2',7'-dichlorodihydrofluorescein diacetate (DCFH-DA; Solarbio, China) in serum-free medium at 37°C for 30 min. Following probe removal and three PBS washes, fluorescence imaging was performed using an inverted epifluorescence microscope (Ti2-U; Nikon, Tokyo, Japan) with

fluorescein isothiocyanate filters (excitation/emission: 488/525 nm). Six random fields per well were captured at 20× magnification under identical exposure settings. Fluorescence intensity was quantified using ImageJ software (v1.53t; NIH, USA) with background subtraction (mean intensity of cell-free wells). Data were normalized against the OA control group (set as 100% ROS level). Three biological replicates with duplicate technical measurements were analyzed.

Intra-Articular Release Analysis

The animal procedures were approved by the Experimental Animal Ethics Committee of the Affiliated Xinhua Hospital of Dalian University (Approval No. 2023–04-01). Twenty-seven 6-week-old male Sprague-Dawley rats (180–200 g) were acclimatized for 7 days under standard housing conditions (22 ± 1°C, 12 h light/dark cycle) with ad libitum access to food and water. Animals were randomly assigned to three treatment groups (n = 9 per group): $MgCl_2$ group, MgO NP group, and $MgO@SiO_2$ group. Under anesthesia induced by intraperitoneal injection of 2.5% tribromoethanol (Sigma-Aldrich, T48402; 1 mL per 100 g body weight), the 50 μL treatments (10 mM Mg^{2+}) were administered via intra-articular injection into the right knee joint. At 1, 3, 5 days post-injection, animals (n = 2 per group per time point) were anesthetized, and synovial fluid was collected via joint lavage: 2 mL sterile deionized water was injected into the articular cavity and aspirated after 30s of gentle articulation. Lavage fluid was centrifuged (10,000 × *g*, 15 min, 4°C), and supernatants were stored at 4°C until analysis. Mg^{2+} concentrations were quantified using ICP-OES. Calibration standards (0.1–20 ppm Mg^{2+} in 2% HNO_3) and spiked recovery samples (85–110%) ensured analytical validity.

Animal Experiments

Nine 6-week-old male Sprague-Dawley rats were acclimatized for 7 days under the aforementioned conditions. Osteoarthritis was induced in the hindlimb knee joint via intra-articular injection of 0.25 mg monosodium iodoacetate (Sigma-Aldrich) dissolved in 50 μL sterile saline.[23] At 1 week post-induction, animals were randomly allocated to three treatment groups (n = 3 per group): sterile saline group (0.9% NaCl), MgO NP group, and $MgO@SiO_2$ group. The 50 μL treatments (5 mM Mg^{2+}) were administered weekly for 4 weeks via intra-articular injection under brief isoflurane anesthesia (3% induction, 1.5% maintenance). Following the 4-week treatment, animals were euthanized via intraperitoneal injection of pentobarbital sodium (150 mg/kg) in accordance with AVMA Guidelines for the Euthanasia of Animals. Knee joints were collected and stored at –20°C for further research.

The knee joints were dissected and fixed in 4% paraformaldehyde at 4°C for 48 h. Macroscopic cartilage degeneration was evaluated using the grading system (0–12 scale) of the Osteoarthritis Research Society International (OARSI), assessing surface integrity (smoothness/ulceration), fissure depth (partial/full-thickness), and erosion extent (0–100% area of involvement) under stereomicroscopy (M205 FA; Leica, Germany).

Histopathological Analysis

Cartilage tissue was decalcified in 10% EDTA at 4°C for 40 days with daily solution replacement. Paraffin-embedded blocks were sectioned coronally at 5 μm thickness using a rotary microtome (RM2235; Leica). Sections underwent hematoxylin and eosin staining following standard protocols. Histopathological scoring was performed by three blinded board-certified pathologists using the OARSI semi-quantitative system (0–7 scale per region), including structural lesioning, chondrocyte density, and cluster formation. Interobserver reliability was confirmed by Cohen's κ coefficient (>0.85). Final scores represent mean values across medial/lateral femoral condyles and tibial plateaus.

Quantification of ROS in Cartilage

Articular cartilage was dissected from femoral condyles and tibial plateaus, rinsed in ice-cold PBS (pH 7.4), and flash-frozen in liquid nitrogen. Tissue samples were homogenized in RIPA lysis buffer (1:10 w/v; Beyotime, China) using a cryogenic grinder (SPEX SamplePrep, USA) at 30 Hz for 2 min. Homogenates were centrifuged at 12,000 × *g* at 4°C for 15 min, and supernatants were aliquoted for analysis. ROS levels were quantified using DCFH-DA following the manufacturer's protocols. Briefly, 50 μL supernatant was incubated with 10 μM DCFH-DA in Hanks' balanced salt solution at 37°C for 30 min in the dark. Fluorescence intensity was measured using a microplate reader (BioTek Synergy H1, USA) with 485/20 nm excitation and 528/20 nm emission filters. Background fluorescence was subtracted using

a reagent blank (DCFH-DA without tissue lysate). Data were normalized against total protein content determined with the BCA assay (Pierce, USA, 23225), with ROS activity expressed as relative fluorescence units per mg protein. Three technical replicates were analyzed per biological sample, and interpolate variability was corrected using internal calibrators.

Immunohistochemical Analysis

Paraffin-embedded cartilage sections (5 μm thickness, prepared as in Quantification of ROS in Cartilage) underwent antigen retrieval by microwave heating (95°C, 15 min) in 10 mM sodium citrate buffer. Endogenous peroxidase activity was quenched with 3% hydrogen peroxide (Sigma-Aldrich) in methanol for 10 min at room temperature. Non-specific binding was blocked by incubation in 3% bovine serum albumin (Sigma-Aldrich) in PBS at 25°C for 1 h. Sections were incubated at 4°C overnight with primary antibodies diluted in the blocking buffer: rabbit anti-IL-6 (1:200; Affinity Biosciences, China), mouse anti-MMP-13 (1:150; Affinity Biosciences), and goat anti-COX-2 (1:300; Affinity Biosciences). After washing with PBS-T (PBS containing 0.1% (w/v) Tween-20), slides were treated with a species-matched horseradish peroxidase–conjugated secondary antibody (1:500; Affinity Biosciences) at 25°C for 1 h. Signal development used 3,3'-diaminobenzidine (Vector Laboratories, USA) with timed incubation (5–10 min), followed by Mayer's hematoxylin counterstaining (30 s; Sigma-Aldrich). Stained sections were imaged under a brightfield microscope (Eclipse Ci-L; Nikon) at 200× magnification.

Statistical Analysis

All quantitative data were analyzed using Prism software (v10.5.0; GraphPad, San Diego, USA). Normality was confirmed via the Shapiro–Wilk test ($\alpha = 0.05$), and homogeneity of variance was assessed with Levene's test. Parametric data are presented as the mean ± standard deviation of ≥3 independent biological replicates. Between-group comparisons for multi-condition experiments were performed using one-way analysis of variance followed by Tukey's post-hoc test for pairwise comparisons. Significance thresholds were defined as $^{*}p < 0.05$ and $^{**}p < 0.01$.

Results and Discussion

$MgO@SiO_2$ nano capsules were synthesized via a modified Stöber method using MgO NPs as the core material. TEM revealed irregularly shaped MgO NPs with a narrow size distribution (18.89 ± 4.58 nm; Figure 1a), consistent with energy dispersive EDS data that confirmed the expected Mg:O atomic ratio of 1:1.38 (41.89% Mg, 58.11% O; Figure 1b). After coating with silica, $MgO@SiO_2$ adopted an irregular spherical morphology with increased mean diameter (49.46 ± 5.4 nm; Figure 1c) and a Mg:Si:O atomic ratio of 1:1.6:5.5 (12.16% Mg, 18.94%Si, 68.90% O; Figure 1d), aligning with prior reports demonstrating silica shell thickness–dependent size modulation.[23] This size range (20–50 nm) is optimal for cellular internalization via clathrin-mediated endocytosis[24] to facilitate, a critical factor for intracellular Mg^{2+} release in chondrocytes. Meanwhile, high-angle annular dark-field imaging (Figure 2a) and cross-sectional EDS mapping (Figure 2b) confirmed the core-shell architecture, with Mg localized centrally and Si distributed peripherally.

Zeta potential measurements in anhydrous ethanol revealed a modest negative surface-charge shift from −8.5 ± 0.4 mV (MgO NPs) to −11.1 ± 0.5 mV ($MgO@SiO_2$; Figure 2c). Although colloidal stability typically requires $|\zeta| > 20$ mV, the mild negative charge may synergize with cartilage's anionic extracellular matrix (rich in glycosaminoglycans) to enhance intra-articular retention via electrostatic repulsion.[25] Finally, X-ray diffraction data (Figure 2d) confirmed characteristic MgO peaks [(111), (200), (220), (311), (222); JCPDS 01–1235] without impurity phases, confirming that crystalline integrity was maintained post-coating. This structural integrity is essential for maintaining the functional properties of MgO, such as its abundant surface area and slow-release ability.[26] Meanwhile, the SiO_2 coating's dual functionality is noteworthy: (1) it mitigates MgO's rapid hydrolysis in aqueous environments, enabling controlled Mg^{2+} release; and (2) its inherent biocompatibility reduces direct interactions between NPs and the plasma membrane, potentially reducing cytotoxicity risk. Indeed, our experimental approach prolonged therapeutic efficacy while minimizing systemic exposure, which is a key advantage over conventional intra-articular therapies that are prone to rapid synovial clearance. These properties position $MgO@SiO_2$ as a promising candidate for sustained chondroprotection in OA management.

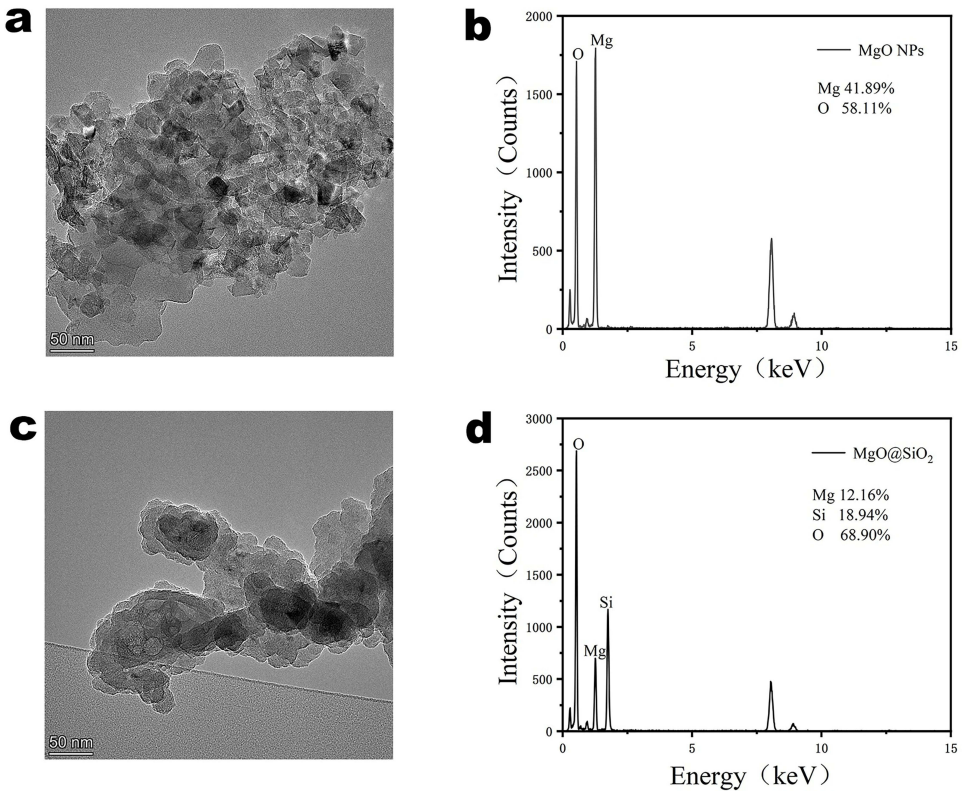

Figure 1 (**a**) TEM image of MgO NPs. (**b**) Elemental composition of MgO NPs, as determined with EDS. (**c**) TEM image of MgO@SiO_2 nano capsules. (**d**): Elemental composition of MgO@SiO_2 nano capsules, as determined with EDS.

As is well known, the biological effects of MgO NPs are intrinsically linked to their local concentration, exhibiting a biphasic "hormetic" response characterized by antioxidative activity at low doses and pro-oxidative effects at higher concentrations.[27] Although this duality enables therapeutic versatility for oncology, antibacterial, anti-inflammatory and anti-aging applications,[28–30] precise control over the release of Mg^{2+} from MgO is critical for OA therapy because excessive ROS generation promotes cartilage degradation whereas inhibiting ROS generation can delay cartilage damage and the inflammatory response caused by OA.[31] Therefore, it is a key strategy to regulate the release of Mg^{2+} from MgO and optimize its advantages as a Mg^{2+} carrier by constructing a composite nanoscale slow-release system. To address this, we engineered SiO_2-coated nanocapsules to modulate MgO dissolution kinetics through physical confinement and surface passivation. Quantitative ICP-OES analysis revealed a MgO content of 89.76 ± 21.46% in bare NPs and 60.83 ± 12.21% in nanocapsules, confirming successful silica encapsulation. This not only verified the authenticity of the MgO material but also suggested that the synthesized MgO@SiO_2 nano capsules would be biologically effective.

The dissolution of MgO-based materials in water can be represented as follows: $MgO + H_2O \rightarrow Mg^{2+} + 2OH^-$. Therefore, the degradation behavior can be indirectly evaluated by monitoring changes in the pH of the solution. In vitro pH monitoring in PBS demonstrated distinct dissolution profiles: bare MgO NPs induced rapid alkalization (pH 10.17 ± 0.12 by day 2) followed by a decline to pH 9.5. ± 0.1 (day 6) due to precipitation of $Mg_3(PO_4)_2$,[32] while MgO@SiO_2 maintained a stable pH (9.57 ± 0.05) through day 6 (Figure 3a). This aligns with silica's known role in retarding hydroxide diffusion through mesoporous channels.[33] Direct Mg^{2+} quantification in deionized water revealed burst release from bare MgO NPs (92.5% ± 0.4 at 24 h) versus sustained release from nanocapsules (91.2% ± 0.3 at 72 h; Figure 3b). These delayed release kinetics matched those reported for silica-gated ion transport in core-shell systems, suggesting tunable release via modulation of shell thickness—a critical advantage for maintaining therapeutic Mg^{2+} concentrations in OA joints.

In vivo intra-articular release profiling revealed critical limitations of conventional Mg^{2+} formulations: $MgCl_2$ showed rapid synovial clearance (0.12 ± 0.02 mg/L) at day 1, consistent with small-molecule efflux through synovial

https://doi.org/10.2147/IJN.S536547

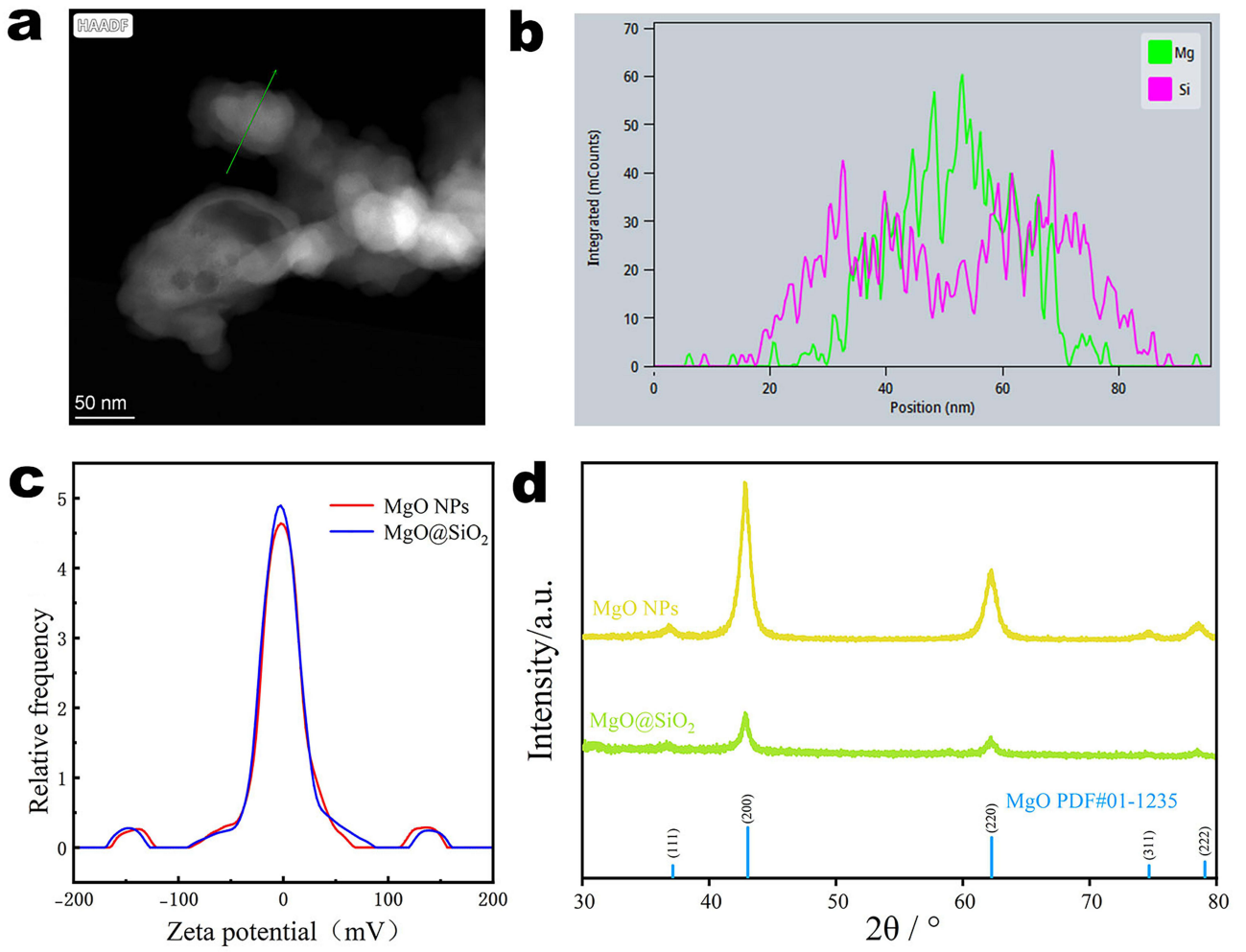

Figure 2 (**a**) High-angle annular dark-field image of $MgO@SiO_2$ sample. (**b**) The cross-sectional elemental analysis was performed with EDS at the green line indicated in panel a. The green spectrum denotes Mg^{2+}, and the pink spectrum denotes Si^{2+}. (**c**) Zeta potential of MgO NPs and $MgO@SiO_2$ samples in anhydrous ethanol. (**d**) X-ray diffraction data MgO NPs and $MgO@SiO_2$ samples.

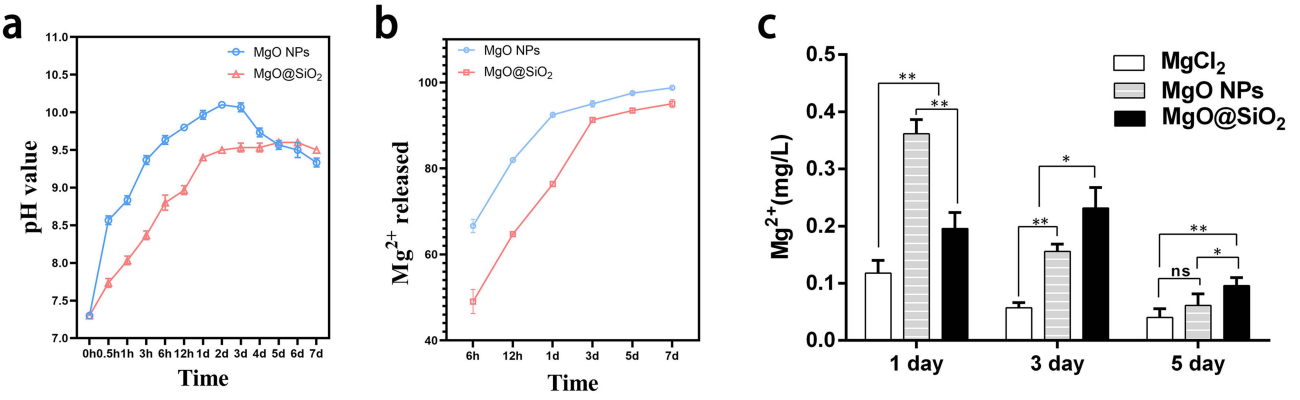

Figure 3 (**a**) Temporal change in pH of MgO NPs or $MgO@SiO_2$ nano capsules immersed in PBS. (**b**) Change in Mg^{2+} concentration when MgO NPs or $MgO@SiO_2$ were immersed in deionized water. (**c**) Release of Mg^{2+} from $MgCl_2$, MgO NPs, and $MgO@SiO_2$ samples in the intraarticular environment. *p < 0.05; **p < 0.01; ns, not significant.

capillaries, as reported.[34] Bare MgO NPs extended retention to 24 h but exhibited premature depletion (0.16 ± 0.01 mg/L vs 0.23 ± 0.04 mg/L for MgO@SiO_2 at day 3; $p < 0.01$), likely owing to phagocytic clearance. Remarkably, MgO@SiO_2 achieved sustained Mg^{2+} levels (0.10 ± 0.01 mg/L) through day 5 (Figure 3c), attributable to the fact that 50-nm particles evade rapid lymphatic drainage, and the negative Zeta potential (−11.1 mV) reduces cartilage adhesion and SiO_2 minimizes opsonization and macrophage uptake. Finally, nanoparticle size is also a key factor for determining the efficiency of nanoparticle uptake via endocytosis. It has been reported that large particles enter cells via phagocytosis, whereas small NPs enter cells through pinocytosis.[35] Therefore, our results provide the first direct evidence for intra-articular MgO dissolution kinetics, addressing a critical gap in nanomaterial-based OA therapeutics. The SiO_2 shell's dual role as a diffusion barrier and biocompatibility enhancer establishes MgO@SiO_2 as a platform technology for joint-targeted sustained release of Mg^{2+}, overcoming limitations of conventional intra-articular injections of $MgCl_2$.

Next, we assessed the biological activity of the nanocapsules. CCK-8 assays revealed concentration-dependent cytotoxicity: bare MgO NPs reduced chondrocyte viability to 63.48% ± 5.35 at 15 mM Mg^{2+} and significantly lower than the bioavailable pool of $MgCl_2$ (88.55% ± 6.91), whereas MgO@SiO_2 maintained >90% bioavailability across all tested concentrations (Figure 4). This demonstrated that the MgO NPs led to higher toxicity at high Mg^{2+} content (15 mM). This difference may be attributed to the ability of higher concentrations of MgO NPs samples to induce ROS production, leading to cytotoxicity.[36] In contrast, MgO@SiO_2 samples did not lead to cytotoxicity because the SiO_2 shell delayed the release of MgO NPs, thus preventing them from reaching concentrations that cause cytotoxicity. Especially at high concentrations, the cell viability in the MgO@SiO_2 samples (94.66% ± 3.25) was higher than that in the $MgCl_2$ samples (88.55% ± 6.91). These results aligned with silica's ability to buffer the dissolution kinetics of MgO NPs, thus preventing Mg^{2+} cytotoxic bursts at high local concentrations.

Subsequently, we examined the effects of different treatments (MgO vs MgO@SiO_2) on the intracellular levels of ROS in OA chondrocytes. The results showed that IL-1β-stimulated chondrocytes exhibited 3.74-fold higher ROS versus blank (87.03 ± 1.64 vs 23.26 ± 0.58; $p < 0.01$; Figure 5a), consistent with published data that ROS production in chondrocytes is one of the main factors leading to the inflammatory response of OA.[37] Interestingly, ROS production in chondrocytes treated with a high concentration of two samples (15 mM) was significantly higher than that in the control. Quantitative analysis demonstrated that ROS in the MgO samples and MgO@SiO_2 samples was 1.14-fold higher (Figure 5b, $p < 0.01$) and 1.09-fold higher (Figure 5c, $p < 0.05$), respectively, than that measured in the control, suggesting that each of these two materials could increase ROS production in OA cells when administered at high concentrations. On the contrary, at 10 mM, both formulations did not significantly increase the ROS level in OA chondrocytes ($p > 0.05$), demonstrating dosage -dependent bioactivity. More importantly, MgO@SiO_2 administered at 5 mM suppressed ROS production to near-baseline levels (1.29-fold vs blank), outperforming bare MgO NPs (1.44-fold), and was significantly lower than that measured for the control group ($p < 0.01$). Both the MgO NPs and MgO@SiO_2 nano capsules exhibited lower average fluorescence intensity at a concentration of 5 mM, demonstrating their statistically

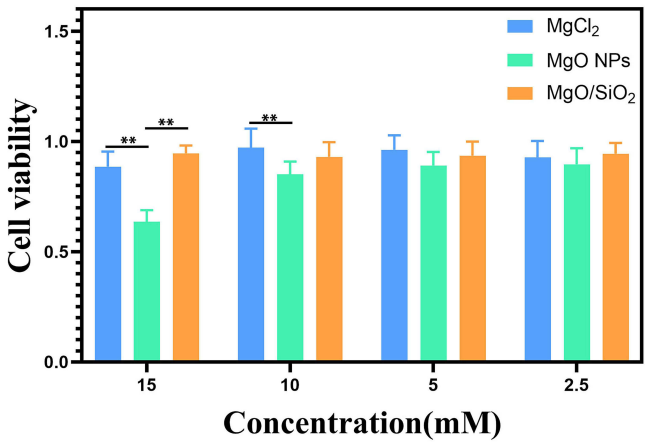

Figure 4 Cytotoxicity of chondrocytes treated with $MgCl_2$, MgO NPs, MgO@SiO_2 nano capsules was evaluated with the CCK-8 assay. **p < 0.01.

https://doi.org/10.2147/IJN.S536547

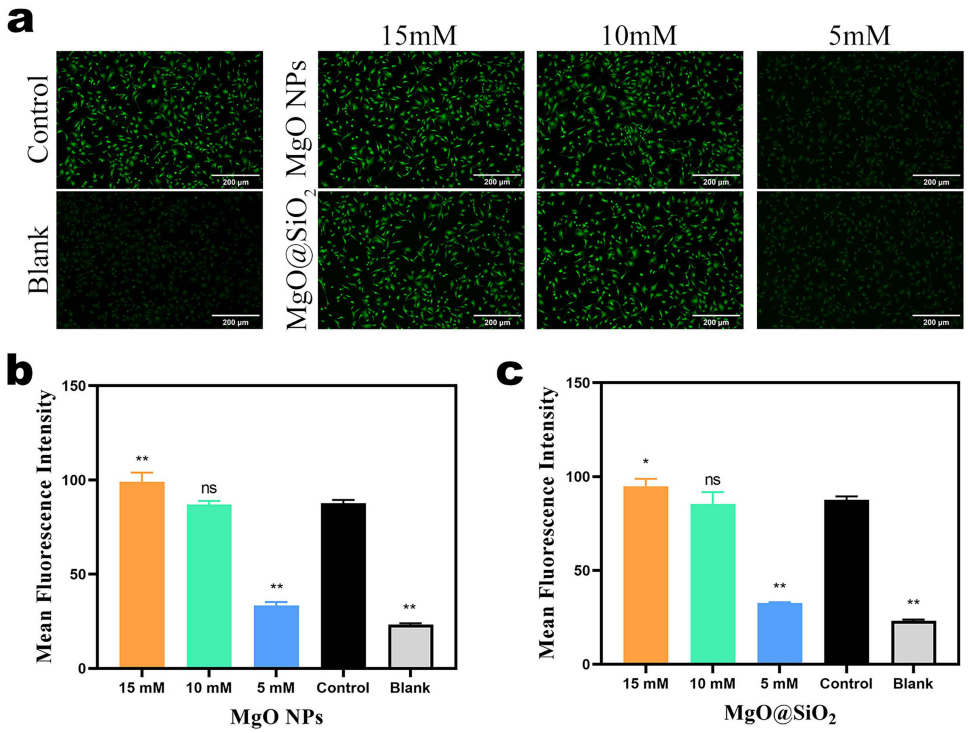

Figure 5 (**a**) Effects of different concentrations of MgO NPs or MgO@SiO_2 nano capsules on ROS production in OA chondrocytes. (**b** and **c**) Fluorescence intensity of ROS in OA chondrocytes treated with different concentrations of MgO NPs (**b**) or MgO@SiO_2 nano capsules (**c**) *p < 0.05 or **p < 0.01 compared with the control group; ns, not significant.

significant ability to reduce ROS levels.[38] Therefore, we chose a concentration of 5 mM for our subsequent animal experiments.

The results of the animal experiments confirmed the results of our in vitro study. Intra-articular administration of MgO@SiO_2 nano capsules (5 mM Mg^{2+}, 4 weeks) markedly attenuated OA progression in rat femoral condyles and tibial plateaus. As shown in Figure 6a, the severity of cartilage erosion and the prevalence of cartilage defects were significantly reduced in the MgO@SiO_2 nano capsule group compared with the other treatment groups, with preservation of articular surface integrity and minimal fissure formation. Moreover, as assessed histologically, the MgO@SiO_2-treated joints exhibited near-normal chondrocyte organization as evidenced by fewer lesions on the condyle surface, decreased loss of glycosaminoglycan (GAG), and increased tissue cellularity and cloning (Figure 6b). Meanwhile, macroscopic evaluation revealed a 50.23% reduction in cartilage erosion score for the MgO@SiO_2 group versus the NaCl control group (23.33 ± 4.72 vs 11.61 ± 1.7; $p < 0.01$; Figure 6c), and the OARSI histological score was 6.0 ± 0.27, which also was significantly lower than that measured for the NaCl control (11.89 ± 0.87; $p < 0.01$; Figure 6d). More importantly, quantification of intracartilaginous ROS demonstrated superior antioxidant efficacy: MgO@SiO_2 reduced ROS to 37.67% ± 1.09 (vs 55.23% ± 2.54 in the NaCl; $p < 0.01$), outperforming bare MgO NPs (47.52% ± 2.0; $p < 0.05$; Figure 6e). This aligned with silica's capacity to sustain a rate of Mg^{2+} release that was below the pro-oxidative threshold (<10 mM), thus minimizing the damage to OA cartilage mediated by ROS oxidative stress. This, it is once again emphasized that ROS clearance is a key mechanism for cartilage protection.

As is well known, an increase in localized ROS concentration is the main cause of chronic inflammation in OA cartilage. When inflammatory mediators such as IL-1β, COX-2 and IL-6 are highly upregulated in OA articular cartilage, they further contribute to ROS production and the expression of MMP-13, leading to the degradation of the cartilage extracellular matrix and hence joint dysfunction.[39] On the contrary, effective clearance of ROS can affect osteoclast differentiation[40] and reduce the expression of proinflammatory factors in OA chondrocytes,[41] thereby protecting chondrocytes and the cartilage matrix. In this study, immunohistochemical profiling revealed the ability of MgO@SiO_2 nano capsules to mediate multimodal suppression of OA-associated mediators: IL-6, MMP-13 and COX-2 expression decreased

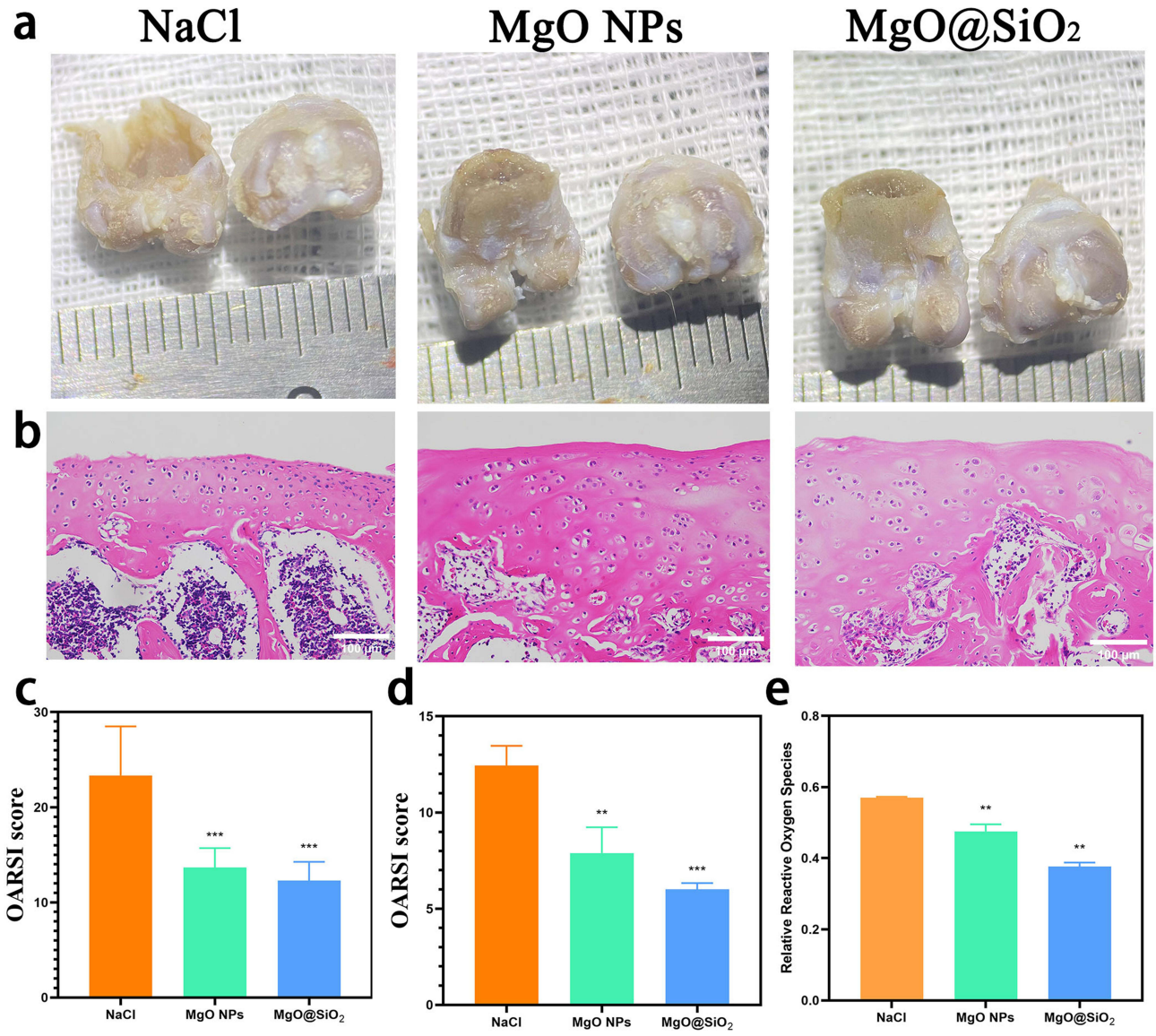

Figure 6 (**a**) Gross appearance of rat knee joints after 4 weeks of treatment with MgO NPs or MgO@SiO_2 nano capsules. (**b**) Images of articular cartilage stained with hematoxylin and eosin. (**c**) Macroscopic OARSI score of knee joints after 4 weeks of treatment. (**d**) Microscopic OARSI score of cartilage based on histological images shown in (**b**). (**e**) ROS levels in cartilage. **p < 0.01; ***p < 0.001.

versus the MgO NPs and control groups (Figure 7). This efficacy stems from the dual capacity of released MgO NPs from nano capsules: its own anti-ROS effect and the ability to facilitate Mg^{2+} release. The SiO_2 shell amplifies these effects by prolonging Mg^{2+} bioavailability, enabling sustained inhibition of the IL-1β-induced activation of proinflammatory Wnt or NF-κB signaling pathways.[3] Notably, the strong correlation between COX-2 reduction and ROS suppression highlights the disruption of the COX-2/ROS axis—a hallmark of OA synovitis.[42] These findings position MgO@SiO_2 as a redox-modulating nanotherapeutic capable of simultaneously targeting multiple pathways involved in OA pathogenesis.

Although our results demonstrate that MgO@SiO_2 nano capsules have therapeutic promise, our study has limitations. First, the particle sizes of our MgO NPs and MgO@SiO_2 nano capsules were small and the particles tended to agglomerate, which may have caused some bias during data acquisition. Further, the single endpoint (4 weeks) precluded analysis of the immune response at earlier times. Finally, the phospholipase activity of human synovial fluid may have altered the kinetics of samples. Therefore, future work should evaluate long-term biocompatibility (>12 weeks) and further clarify the pathways regulated by Mg^{2+}.

https://doi.org/10.2147/IJN.S536547

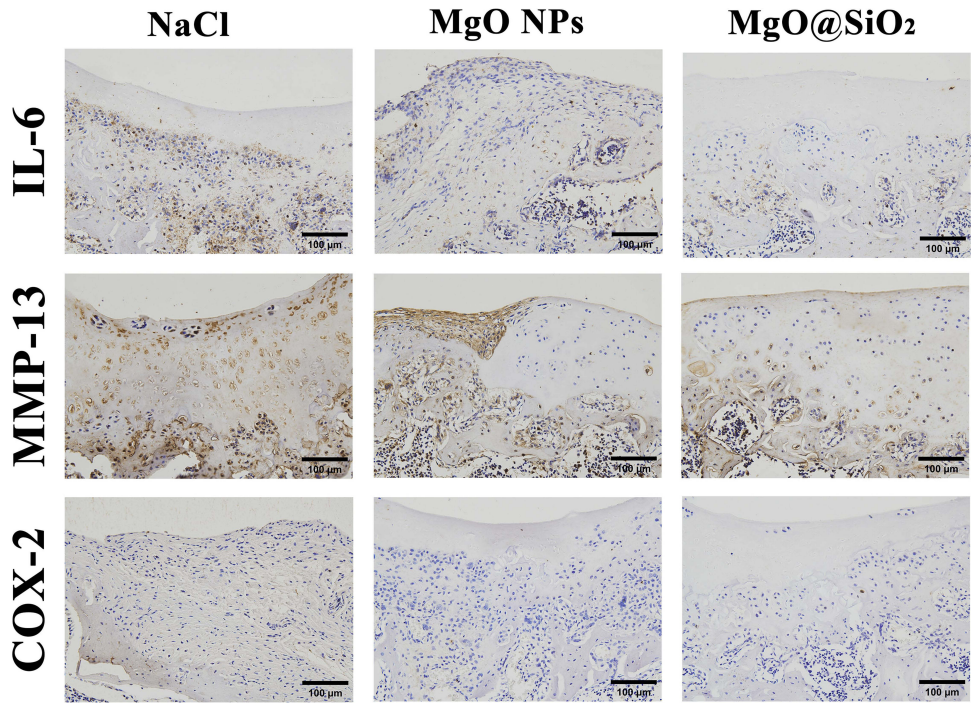

Figure 7 Images of immunohistochemical staining for cytokines (IL-6, MMP-13, and COX-2) in OA articular cartilage after 4 weeks of [treatment with MgO NPs or $MgO@SiO_2$ nanocapsules.

Conclusion

Our research establishes $MgO@SiO_2$ nano capsules as a novel OA therapeutic agent and that the kinetics of Mg^{2+} release from MgO NPs (both in vitro and in vivo) is prolonged by the silica shell on the surface of the $MgO@SiO_2$ nanocapsules. Notably, our data confirm that low-concentration administration of $MgO@SiO_2$ nano capsules has the advantages of controlled release, targeted therapy, and high loading rate, especially for alleviating OA cartilage injury by clearing ROS and inhibiting the expression of proinflammatory factors in cartilage tissue. Therefore, as a multi-functional ROS-responsive nanosystem, $MgO@SiO_2$ nano capsules not only can alleviate the clinical symptoms of OA but also provide a new option for slowing or reversing OA pathology, which will help further clarify the promotion and application of nanocapose technology in the field of OA therapy. In additional, by resolving the conflict between magnesium's therapeutic duality and the limitations on its clearance from joints, the $MgO@SiO_2$ nano capsules we describe will enable long-term intra-articular Mg^{2+} release and hence supplementation of the local Mg^{2+} concentration —a strategy with implications for other ion-deficiency arthropathies.

Acknowledgments

This work was financially supported by funds from the Interdisciplinary Project of Dalian University (DLUXK-2023-YB -008), Key Discipline Project of Affiliated Xinhua Hospital of Dalian University (2022003), and LiaoNing Revitalization Talents Program (Grant No. XLYC2403047).

Author Contributions

All authors have read and approved the paper.

Disclosure

All authors declare that no conflict of interest exists in the submission of this paper.

References

1. Hunter DJ, Bierma-Zeinstra S. Osteoarthritis. *Lancet*. 2019;393(10182):1745–1759. doi:10.1016/S0140-6736(19)30417-9

2. Courties A, Kouki I, Soliman N, Mathieu S, Sellam J. Osteoarthritis year in review 2024: epidemiology and therapy. *Osteoarthritis Cartilage*. 2024;32(11):1397–1404. doi:10.1016/j.joca.2024.07.014
3. Yao Q, Wu X, Tao C, et al. Osteoarthritis: pathogenic signaling pathways and therapeutic targets. *Signal Transduct Target Ther*. 2023;8(1):56. doi:10.1038/s41392-023-01330-w
4. Chen Y, Zhang Y, Wu C, et al. High-throughput screening strategy and metal-organic framework-based multifunctional controlled-release nanomaterial for osteoarthritis therapy. *ACS Nano*. 2025;19(4):4802–4819. doi:10.1021/acsnano.4c15740
5. An X, Yu W, Liu J, Tang D, Yang L, Chen X. Oxidative cell death in cancer: mechanisms and therapeutic opportunities. *Cell Death Dis*. 2024;15(8):556. doi:10.1038/s41419-024-06939-5
6. Goudarzi R, Dehpour AR, Partoazar A. Nanomedicine and regenerative medicine approaches in osteoarthritis therapy. *Aging Clin Exp Res*. 2022;34(10):2305–2315. doi:10.1007/s40520-022-02199-5
7. Todd T, Lu Z, Zhao J, et al. LiF@SiO2 nanocapsules for controlled lithium release and osteoarthritis treatment. *Nano Res*. 2018;11(10):5751–5760. doi:10.1007/s12274-018-2061-5
8. Abdel-Aziz MA, Ahmed HMS, El-Nekeety AA, Sharaf HA, Abdel-Aziem SH, Abdel-Wahhab MA. Biosynthesis of gold nanoparticles for the treatment of osteoarthritis alone or in combination with Diacerein® in a rat model. *Inflammopharmacology*. 2021;29(3):705–719. doi:10.1007/s10787-021-00833-8
9. Zhao X, Huang H, Jiang X, et al. Supramolecular nanoparticle loaded with bilirubin enhances cartilage protection and alleviates osteoarthritis via modulating oxidative stress and inflammatory responses. *Colloids Surf B Biointerfaces*. 2025;245:114243. doi:10.1016/j.colsurfb.2024.114243
10. Peng Y, Yang Z, Li J, Liu S. Research progress on nanotechnology of traditional Chinese medicine to enhance the therapeutic effect of osteoarthritis. *Drug Deliv Transl Res*. 2024;14(6):1517–1534. doi:10.1007/s13346-024-01517-w
11. Li Z, Zheng X, Wang Y, et al. The biomimetics of Mg2+-concentration-resolved microenvironment for bone and cartilage repairing materials design. *Biomimetic*. 2022;7(4):227. doi:10.3390/biomimetics7040227
12. Li Y, Yue J, Yang C. Unraveling the role of Mg(++) in osteoarthritis. *Life Sci*. 2016;147:24–29. doi:10.1016/j.lfs.2016.01.029
13. Bondok RS, Abd El-Hady AM. Intra-articular magnesium is effective for postoperative analgesia in arthroscopic knee surgery. *Br J Anaesth*. 2006;97(3):389–392. doi:10.1093/bja/ael176
14. Yao H, Xu JK, Zheng NY, et al. Intra-articular injection of magnesium chloride attenuates osteoarthritis progression in rats. *Osteoarthritis Cartilage*. 2019;27(12):1811–1821. doi:10.1016/j.joca.2019.08.007
15. Đurić V, Petrović J, Stanić D, Ivanović A, Kotur-Stevuljević J, Pešić V. Magnesium suppresses in vivo oxidative stress and ex vivo DNA damage induced by protracted ACTH treatment in rats. *Magnes Res*. 2023;36(1):1–13. doi:10.1684/mrh.2023.0510
16. Wang N, Maskomani S, Meenashisundaram GK, Fuh JYH, Dheen ST, Anantharajan SK. A study of Titanium and Magnesium particle-induced oxidative stress and toxicity to human osteoblasts. *Mater Sci Eng C Mater Biol Appl*. 2020;117:111285. doi:10.1016/j.msec.2020.111285
17. Kwesiga MP, Gillette AA, Razaviamri F, et al. Biodegradable magnesium materials regulate ROS-RNS balance in pro-inflammatory macrophage environment. *Bioact Mater*. 2022;23:261–273. doi:10.1016/j.bioactmat.2022.10.017
18. Zhang L, Wang Z, Lu T, et al. Mitochondrial Ca2+ overload leads to mitochondrial oxidative stress and delayed meiotic resumption in mouse oocytes. *Front Cell Dev Biol*. 2020;8:580876. doi:10.3389/fcell.2020.580876
19. Liu M, Zhang W, Chen Z, et al. Mechanisms of magnesium oxide-incorporated electrospun membrane modulating inflammation and accelerating wound healing. *J Biomed Mater Res A*. 2023;111(1):132–151. doi:10.1002/jbm.a.37453
20. Lu S, Zhu Y, Lin J, Li Y, Wu L. Controlled delivery of procyanidin through magnesium oxide nanoparticles (MgO NPs) to improve the activity and mineralization of osteoblasts under oxidative stress in vitro. *Biomed Mater*. 2024;19(4). doi:10.1088/1748-605X/ad5260
21. Mei S, Jiang F, Liu N, et al. Sol-gel synthesis of magnesium oxide nanoparticles and their evaluation as a therapeutic agent for the treatment of osteoarthritis. *Nanomedicine*. 2024;19(23):1867–1878. doi:10.1080/17435889.2024.2382421
22. Liu N, Jiang F, Feng Z, et al. MgO@SiO2 nanocapsules:A controlled magnesium ion release system for targeted inhibition of osteoarthritis progression. *Nanoscale Adv*. 2025;7:1814–1824. doi:10.1039/D4NA00900B
23. Ju L, Hu P, Chen P, et al. Huoxuezhitong capsule ameliorates monosodium iodoacetate–induced osteoarthritis of rats through suppressing PI3K/Akt/ NF-κB pathway. *Biomed Pharmacother*. 2020;129:110471. doi:10.1016/j.biopha.2020.110471
24. Salatin S, Maleki Dizaj S, Yari Khosroushahi A. Effect of the surface modification, size, and shape on cellular uptake of nanoparticles. *Cell Biol Int*. 2015;39(8):881–890. doi:10.1002/cbin.10459
25. Li W, Liu X, Sun L, et al. Effects of physicochemical properties of nanomaterials on their toxicity. *J Biomed Mater Res A*. 2015;103(7):2499–2507. doi:10.1002/jbm.a.35384
26. Shim KH, Hulme J, Maeng EH, Kim MK, An SS. Analysis of SiO2 nanoparticles binding proteins in rat blood and brain homogenate. *Int J Nanomed*. 2014;9 Suppl 2:207–215. doi:10.2147/IJN.S58203
27. Venkatappa MM, Udagani C, Hanumegowda SM, et al. Effect of biofunctional green synthesized mgo-nanoparticles on oxidative-stress-induced tissue damage and thrombosis. *Molecules*. 2022;27(16):5162. doi:10.3390/molecules27165162
28. Sambandam T, Karuppasamy G, Perumal G, Rajasingh EC. Liquid phase preparation and characterization of MgO nanoparticles and their butchery activities against dental bacterial pathogens and human cervical cancer cell line. *J Photochem Photobiol B*. 2025;262:113084. doi:10.1016/j.jphotobiol.2024.113084
29. Nguyen NTT, Nguyen LM, Nguyen TTT, Tran UPN, Nguyen DTC, Tran TV. A critical review on the bio-mediated green synthesis and multiple applications of magnesium oxide nanoparticles. *Chemosphere*. 2023;312(Pt 1):137301. doi:10.1016/j.chemosphere.2022.137301
30. Jahangiri L, Kesmati M, Najafzadeh H. Evaluation of analgesic and anti-inflammatory effect of nanoparticles of magnesium oxide in mice with and without ketamine. *Eur Rev Med Pharmacol Sci*. 2013;17(20):2706–2710.
31. Xue C, Tian J, Cui Z, et al. Reactive oxygen species (ROS)-mediated M1 macrophage-dependent nanomedicine remodels inflammatory microenvironment for osteoarthritis recession. *Bioact Mater*. 2023;33:545–561. doi:10.1016/j.bioactmat.2023.10.032
32. Zheng L, Zhao S, Li Y, et al. Engineered MgO nanoparticles for cartilage-bone synergistic therapy. *Sci Adv*. 2024;10(10):eadk6084. doi:10.1126/sciadv.adk6084
33. Halevas E, Mavroidi B, Nday CM, et al. Modified magnetic core-shell mesoporous silica nano-formulations with encapsulated quercetin exhibit anti-amyloid and antioxidant activity. *J Inorg Biochem*. 2020;213:111271. doi:10.1016/j.jinorgbio.2020.111271
34. Jin GZ. Current nanoparticle-based technologies for osteoarthritis therapy. *Nanomaterials*. 2020;10(12):2368. doi:10.3390/nano10122368

35. Hadji H, Bouchemal K. Effect of micro- and nanoparticle shape on biological processes. *J Control Release*. 2022;342:93–110. doi:10.1016/j.jconrel.2021.12.032
36. Kumaran RS, Choi YK, Singh V, et al. In vitro cytotoxic evaluation of MgO nanoparticles and their effect on the expression of ROS genes. *Int J Mol Sci*. 2015;16(4):7551–7564. doi:10.3390/ijms16047551
37. Arra M, Swarnkar G, Ke K, et al. LDHA-mediated ROS generation in chondrocytes is a potential therapeutic target for osteoarthritis. *Nat Commun*. 2020;11(1):3427. doi:10.1038/s41467-020-17242-0
38. Podder S, Chanda D, Mukhopadhyay AK, et al. Effect of morphology and concentration on crossover between antioxidant and pro-oxidant activity of MgO nanostructures. *Inorg Chem*. 2018;57(20):12727–12739. doi:10.1021/acs.inorgchem.8b01938
39. Ansari MY, Ahmad N, Haqqi TM. Oxidative stress and inflammation in osteoarthritis pathogenesis: role of polyphenols. *Biomed Pharmacother*. 2020;129:110452. doi:10.1016/j.biopha.2020.110452
40. Jeon S, Min Kim T, Kwon G, et al. Targeting ROS in osteoclasts within the OA environment: a novel therapeutic strategy for osteoarthritis management. *J Tissue Eng*. 2024;15:20417314241279935. doi:10.1177/20417314241279935
41. Zhang Z, Zhang N, Li M, Ma X, Qiu Y. Sappanone a alleviates osteoarthritis progression by inhibiting chondrocyte ferroptosis via activating the SIRT1/Nrf2 signaling pathway. *Naunyn Schmiedebergs Arch Pharmacol*. 2024;397(11):8759–8770. doi:10.1007/s00210-024-03179-4
42. Liu C, Chen Y. Ketorolac tromethamine alleviates IL-1β-induced chondrocyte injury by inhibiting COX-2 expression. *Exp Ther Med*. 2022;23(5):337. doi:10.3892/etm.2022.11267